Unravelling the magnetic signal of individual grains in a Hawaiian lava using Micromagnetic Tomography

Martha E Kosters[1], Rosa A de Boer[1], Frenk Out[1], David Ignacio Cortés-Ortuño[1], and Lennart Vincent de Groot[1]

[1]Utrecht University

November 23, 2022

Abstract

Micromagnetic Tomography (MMT) is a new technique that allows to determine magnetic moments of individual grains in volcanic rocks. Current MMT studies either showed that it is possible to obtain magnetic moments of relatively small numbers of grains in ideal sample material, or provided important theoretical advances in MMT inversion theory and/or its statistical framework. Here we present a large-scale application of MMT on a sample from the 1907-flow from Hawaii's Kilauea volcano producing magnetic moments of 1,646 individual grains. To assess the robustness of the MMT results, we produced 261,305 individual magnetic moments in total: an increase of three orders of magnitude compared to earlier studies and a major step towards the number of grains that is necessary for paleomagnetic applications of MMT. Furthermore, we show that the recently proposed signal strength ratio is a powerful tool to scrutinize and select MMT results. Despite this progress, still only relatively large iron-oxide grains with diameters >1.5-2 µm can be reliably resolved, impeding a reliable paleomagnetic interpretation. To determine the magnetic moments of smaller (< 1 µm) grains that may exhibit PSD behavior and are therefore better paleomagnetic recorders, the resolution of the MicroCT and magnetic scans necessary for MMT must be improved. Therefore, it is necessary to reduce the sample size in future MMT studies. Nevertheless, our study is an important step towards making MMT a useful paleomagnetic and rock-magnetic technique.

Unravelling the magnetic signal of individual grains in a Hawaiian lava using Micromagnetic Tomography

Martha E. Kosters[1]*, Rosa A. de Boer[1], Frenk Out[1], David I. Cortés-Ortuño[1], Lennart V. de Groot[1]*.

[1] Paleomagnetic laboratory Fort Hoofddijk, dept of Earth Sciences, Utrecht University, Budapestlaan 17, 3584 CD Utrecht, the Netherlands

* Corresponding author: Lennart de Groot (l.v.degroot@uu.nl)

Key points:

- We studied a sample from the 1907-flow of Kilauea (Hawaii) with well-known rock-magnetic properties with Micromagnetic Tomography (MMT)
- We performed 16,874 MMT inversions to characterize the magnetic moments of 1,646 grains resulting in 261,305 unique magnetic moments
- Magnetic moments were only found for grains >1.5-2 µm that exhibit multidomain behavior, but these MMT results are statistically robust

Keywords

Micromagnetic Tomography, Rock-magnetism, Magnetic mineralogy, MicroCT analysis, Quantum Diamond Microscope, Micromagnetic inversions

Abstract

Micromagnetic Tomography (MMT) is a new technique that allows to determine magnetic moments of individual grains in volcanic rocks. Current MMT studies either showed that it is possible to obtain magnetic moments of relatively small numbers of grains in ideal sample material, or provided important theoretical advances in MMT inversion theory and/or its statistical framework. Here we present a large-scale application of MMT on a sample from the 1907-flow from Hawaii's Kilauea volcano producing magnetic moments of 1,646 individual grains. To assess the robustness of the MMT results, we produced 261,305 individual magnetic moments in total: an increase of three orders of magnitude compared to earlier studies and a major step towards the number of grains that is necessary for paleomagnetic applications of MMT. Furthermore, we show that the recently proposed signal strength ratio is a powerful tool to scrutinize and select MMT results. Despite this progress, still only relatively large iron-oxide grains with diameters >1.5-2 µm can be reliably resolved, impeding a reliable paleomagnetic interpretation. To determine the magnetic moments of smaller (< 1 µm) grains that may exhibit PSD behavior and are therefore better paleomagnetic recorders, the resolution of the MicroCT and magnetic scans necessary for MMT must be improved. Therefore, it is necessary to reduce the sample size in future MMT studies. Nevertheless, our study is an important step towards making MMT a useful paleomagnetic and rock-magnetic technique.

Plain language summary

The magnetic information of volcanic rocks is an invaluable archive of the behavior of the Earth's magnetic field through time. Recently a new technique was proposed, Micromagnetic Tomography, that promises to determine magnetic signals of individual iron-bearing grains in these rocks. This would greatly improve our ability to obtain and interpreted the magnetic information stored in them. Here we go beyond the proof-of-concept of this exciting new technique and show that it is indeed possible to obtain statistically robust results for set of rather large grains, with diameters >1.5-2 µm, in a sample from the 1907-flow from Hawaii's Kilauea volcano.

1. Introduction

Geological materials and archeological artefacts containing magnetic particles record the direction and intensity of the past geomagnetic field as they cool. These thermoremanent magnetizations (TRMs) are our primary source of information on the behavior of the Earth's magnetic field. Obtaining reliable paleointensities and paleodirections from samples with a large variation in grainsizes is a challenge, due to differences in magnetic behavior between grains that differ in size, shape, and chemistry (e.g. Dunlop and Özdemir, 1997; Tauxe and Yamazaki, 2015). In paleomagnetic measurement techniques that rely on bulk measurements, the contributions of individual grains are measured collectively, i.e. the signals of many millions of grains result in a single magnetic moment for the entire sample. This possibly obscures information from grains that record the paleofield well by the signal of non-perfect recorders in the sample. Especially the presence of large (>>1µm), multidomain (MD), grains often prevent a reliable interpretation of a magnetic signal from a bulk sample. Samples consisting of predominantly single-domain (SD) grains or slightly larger (but <1 µm) pseudo-single domain (PSD) grains with complex domain structures such as vortices or 'flower states' generally produce more reliable paleomagnetic data (e.g. Nagy et al., 2017; 2019).

Over the past decades, a number of studies have focused on high-end magnetometry techniques to assess the magnetic state of magnetic recorders and micromagnetic processes in them on a (sub) micrometer scale (e.g. Almeida et al., 2016; Farchi et al., 2017; Lima & Weiss, 2009; Nichols et al., 2016; Weiss et al., 2007). These magnetometry techniques, such as scanning SQUID microscopy (Egli and Heller 2000; Weiss et al. 2007; Lima and Weiss 2016), Electron Holography (Harrison et al. 2002; Feinberg et al. 2006; Almeida et al. 2016), and the Quantum Diamond Microscope (Glenn et al. 2017; Levine et al. 2019; Fu et al. 2020) allow to zoom in on individual grains or magnetically well-behaved small regions in a sample, and thus can avoid magnetically adverse behaved regions or grains.

The recently developed Micromagnetic Tomography method (MMT, de Groot et al. 2018; 2021) builds on this collection of magnetometry techniques. MMT proposes to overcome the differences in recording properties between grains of various sizes in a bulk sample, by separating the contributions of individual grains to the bulk magnetic signal. It relies on supplementing the results of scanning magnetometry on the surface of a sample with spatial data of the magnetic recorders within a non-magnetic matrix. This enables a three-dimensional interpretation of the magnetometry through a least-squares inversion that allocates magnetizations to individual magnetic grains. The spatial data on the magnetic recorders is acquired from X-ray computed tomography (MicroCT) scans.

As recognized by de Groot et al. (2021), the development of MMT is promising, but currently there are major challenges left to solve before MMT can be routinely used for paleomagnetic and rock-magnetic studies. Most previous MMT studies used synthetic samples and produced results for a limited amount of grains (<150) in them. Here we present the first results from MMT applied to a natural volcanic sample. We show (1) that it is possible to determine magnetic moments for large, MD, grains in our sample, (2) that the current computational setup is capable of solving for a statistically relevant number of grains and (3) which challenges currently remain and will be the topic of future research. Despite our progress, our MMT results cannot yet be interpretated in paleomagnetic terms because we only solve for the moment of large, MD, grains. To obtain information from the paleomagnetically more relevant, PSD, grains, the resolution of the MicroCT scan used must be increased. Nevertheless, our study provides an insight into how the development of MMT for paleomagnetic uses can progress, and we illustrate how MMT data can be scrutinized and selected based on the recently proposed statistical framework by Out et al. (2022).

2. Sample description

For this study we selected material from the 1907 lava flow of Kilauea, Hawaii. This material was sampled as site HW03 (de Groot et al. 2013), and its rock-magnetic properties were described in depth (Ter Maat at al. 2018). Our sample is a cylindrical cutout from a thin section with a sample layer of 30 µm thick, with a diameter of 3 mm. The same sample was already used for one of the case studies in de Groot et al. (2021). HW03 consists of tholeiitic basalt with minor alteration, consisting of a low percentage (< 5%) iron-oxides.

2.1 Petrography

The iron-oxides are copious and present throughout the sample. They are <30 µm in size, have a cubic shape and have experienced minor oxyexsolution (Fig. 1 and Ter Maat et al. 2018). A micrograph of the thin section shows that the sample contains areas with a lower number of relatively large iron-oxide grains (> 3µm, 'A' in Fig. 1a) and areas with a higher number of relatively small (< 3 µm, 'B' in Fig. 1a) iron oxide grains. The circular cut-out that was used for this study contains an area with mainly relatively large grains, and thus not so many of them. The material surrounding the iron-oxide grains has a porphyritic structure with large (100-200 µm) clinopyroxene and plagioclase crystals and contains some equant olivine phenocrysts. The remaining material mainly consists of fine-grained clinopyroxene, plagioclase, and glass (Fig. 1b, c, and d).

2.2 Chemical and magnetic analysis

Ter Maat et al. (2018) chemically analyzed 22 iron-oxide grains from HW03 using a microprobe. Based on the microprobe analysis the grains can be roughly divided in two mineralogical families. The first mineralogical family is ilmenite with a relatively equal Ti and Fe content of ~19 atom% each (6 grains). The other family is titanomagnetite with a high Fe and low Ti content varying in ratio from 3:1 to 7:1 (15 grains). Lastly, there is one grain of which two spot readings show that it is partly ilmenite and partly titanomagnetite. Further investigation by Scanning Electron Microscope (SEM) using Backscatter Electrons (BSE) to characterize the crystallographic lattice shows mineralogical domains within grains that are either titanomagnetite (cubic) or ilmenite (hexagonal). Within these mineralogical domains magnetic domains can exist, but it is important to keep in mind that ilmenite is paramagnetic and titanomagnetite is ferrimagnetic at room temperature (Readman and O'Reilly 1972), i.e. only the titanomagnetite grains may hold a remanent magnetization. Investigation by Magnetic Force Microscopy (MFM) of four grains indeed showed multiple magnetic domains within

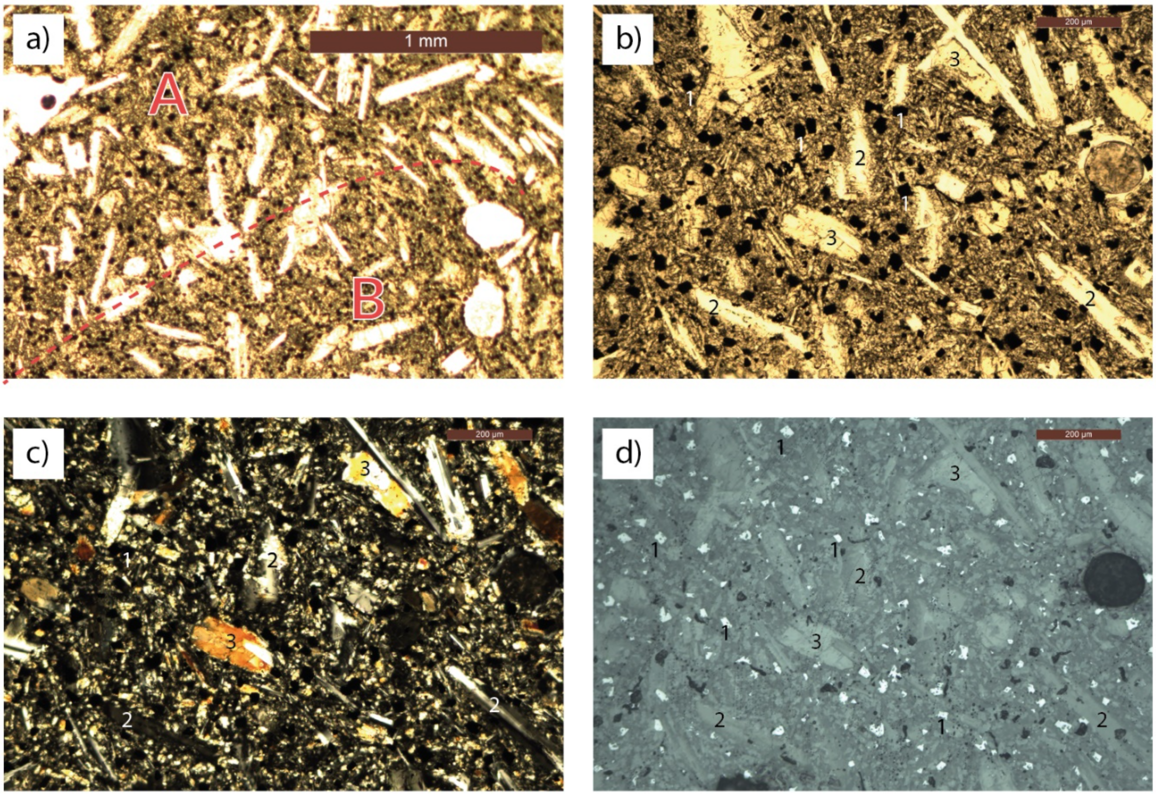

Figure 1 - Petrology and minerology of HW-03. Panel a shows a portion of the sample under plane polarized light (PPL) in which two areas A and B are loosely defined. Area A is an area with a sparse amount of large magnetite grains and area B an area with a higher density of smaller magnetite grains. The magnification in panels b, c, and d is larger and show the sample under PPL, crossed polarized light (XPL) and reflected light, respectively. Each shows the same field of view in which the different minerals are indicated: magnetite (1), clinopyroxene (2) and plagioclase (3). The cubic nature of the magnetite grains is especially visible under reflected light (d).

the titanomagnetite mineralogical domains (Ter Maat et al. 2018), but no magnetic signal in the ilmenite part of this particular grain. As it is currently impossible to discriminate between ilmenite and titanomagnetite in the MicroCT scans used to characterize the iron-oxides for our MMT study, some (parts) of the grains selected by the MicroCT analyses do not have a magnetic signal at room temperature.

3. Methods

The MMT method relies on combining spatial information of the location and shape of individual magnetic grains with the magnetic surface expressions of those same grains to solve their individual magnetic moments (de Groot et al. 2018; 2021). Supplementing the magnetic surface scan with spatial information is necessary to overcome the traditional non-uniqueness in potential field inversion problems (Fabian and de Groot 2019).

3.1 Spatial data acquisition

The spatial information is derived from MicroCT scans that produce a three-dimensional image of the X-ray attenuation contrast in a sample that is often interpreted in terms of variations in density in the sample (e.g. Sakellariou et al. 2004). The interpretation of the three-dimensional image relies on the large attenuation contrast between the highly dense magnetic grains and the lower density surrounding matrix. Using a threshold, voxels with high density are retained, voxels with low density removed. Subsequently, adjacent, interconnected, high density voxels are grouped together to form a grain, for which the size, shape, and location are known. From this data physical properties such as volume and the distance to the surface can be calculated for each grain individually. The sample for this study was imaged by the Nanotom-S MicroCT at TU Delft. The scan had a resolution of 0.75 µm (voxelsize: 0.75x0.75x0.75 µm) and a field of view of 1901x2301 pixels. To suppress noise, grains that consist of 10 voxels or less were discarded, which inherently implies that the smallest grains included in the inversion routine are approximately 1.5-2 µm in diameter. This is a major shortcoming of our MMT study, as smaller grains are undoubtedly present in our sample and are usually assumed to the be most reliable magnetic recorders. Also, it is important for the inversion routine that all magnetic sources in the system are known, otherwise there are magnetic contributions in the surface magnetometry that cannot be attributed to their source. Missing grains with diameters <1.5-2 µm will therefore lead to less reliable MMT results. Nevertheless, the mineralogical investigation of this sample shows that many grains in our sample are >3 µm. Furthermore, a major part of the discussion of this paper consists of assessing how well the grains that are detected by our MicroCT scan are resolved, in spite of missing smaller grains in our sample and other sources of uncertainty.

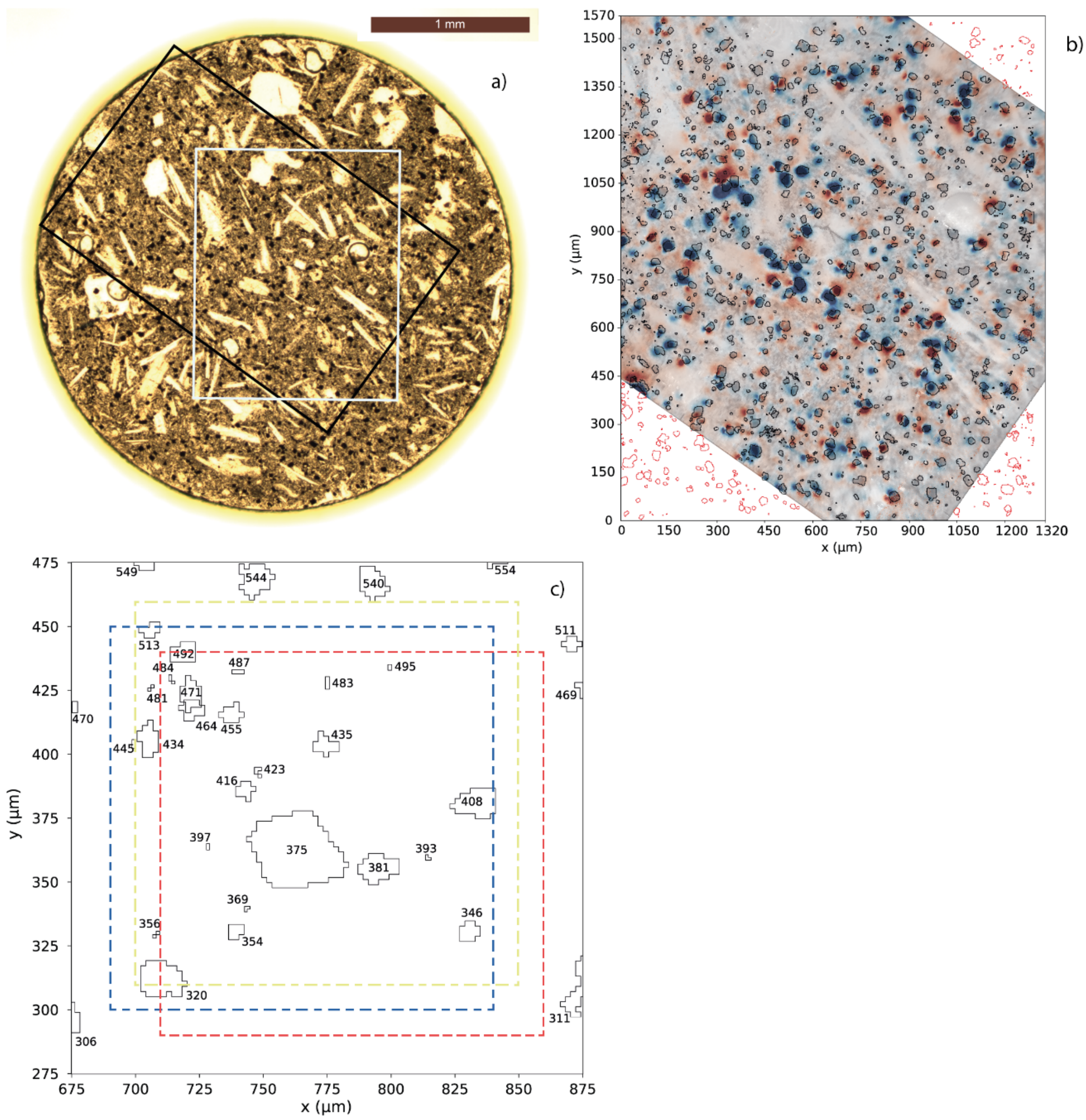

Figure 2 - The mapping of the QDM and MicroCT-scans. Panel a shows a microscope image of the entire sample, with the MicroCT field-of-view outlined in white and the QDM's field-of-view in black. In panel b the magnetic scan of the QDM is in the background (positive flux in blue, negative in red, an absolute scale lacks due to distortion from the other layer in the image), overlain by the QDM's LED image in 50% transparency. The grains as obtained from the MicroCT scan are outlined in black when they are in the QDM's field-of-view, in red when they are outside. Three unique subareas are shown in panel c, each subarea is 150 x 150 μm and they are spaced at 10 μm intervals. The horizontal (x) and vertical (y) axes in panels b and c have the same origin and are in μm. The exclusion of grains due to intersecting the boundary of a subarea is illustrated by e.g. grain 513: it will be included in the blue and yellow subareas during the inversion but its results in the blue subarea will be discarded after the inversion was performed, because it intersects the boundary of the subarea.

3.2 Magnetic surface flux

The surface magnetizations for MMT can be imaged using a variety of instruments and techniques (as summarized in de Groot et al. (2021). The sample in our study was imaged by a Quantum Diamond Microscope (QDM) at Harvard (Glenn et al. 2017). The QDM determines the magnetic flux above the surface of a sample by measuring (dips in) fluorescence arising from nitrogen-vacancy (NV) centers in a diamond chip. The magnetic data is thus acquired from an optical image with a field of view of 1920x1200 pixels and a spatial resolution of 1.2 µm. During operation a 0.9 mT bias field is applied; its polarity is switched many times during measurement. Potentially induced (paramagnetic) magnetization in the sample can be removed from the remanent (ferrimagnetic) part of the signal by taking the average of the images acquired with switched polarity. The coercivities of naturally occurring iron-oxide grains are generally >>0.9 mT (Readman and O'Reilly 1972; Dunlop and Özdemir 1997); this bias field therefore would not prevent a paleomagnetic interpretation of QDM results.

3.3 Co-registration

The two datasets must be co-registered in the same coordinate system to apply the inversion routine. The QDM is an optical acquisition technique, and its camera can also be used to optically image the surface of the sample in the same coordinates as the magnetic scan. The MicroCT data can be sliced to only show the grains close to the surface of the sample. This enables co-registration based on the geometry of shallow grains (Fig. 2a). Since the two scans do not overlap entirely, not all grains imaged by the MicroCT have a co-registered magnetic flux signal (Fig. 2b). In total 1,646 grains were imaged by both the MicroCT and QDM analyses. Also, the scan height, i.e. the sample-sensor distance needs to be precisely known to properly co-register the MicroCT and QDM datasets. This distance was 6.0 µm and is derived from the actuators of the QDM set-up.

3.4 Inversion set-up

The inversion routine is identical to the inversion scheme used in (de Groot et al. 2018; 2021) and based on the theory in (Fabian and de Groot 2019). The data in those publications was processed on a desktop computer and performing the inversion routine for one area of 150x150 µm with the grain density of our sample took approximately 2 weeks computational time. For this study, the inversion routine was highly optimized and moved to Python to use state-of-the-art libraries. Furthermore, we now use a computational server with 52 double-threaded cores and 192 GB RAM. These improvements allow to perform a single inversion of an area of 150x150 µm in approximately 1.5 minutes. Because the inversion has a high RAM demand, the size of the area that can be inverted in one calculation is still limited to 150x150 µm. Therefore, to analyze the entire sample, it is inverted in many overlapping subareas: so called 'tiling' (Fig. 2c). The subareas have an interspacing of 10 µm, leading to 118 subareas to be inverted along the x-axis and 143 subareas along the y-axis, so there are 16,874 subareas in total. Tiling, however, has drawbacks. First, the inversion in subareas implies that grains can be intersected by the subarea boundary. A boundary condition of the inversion is that all magnetic sources in the system and their magnetic signals are imaged, and no sources or signals are missed. The inversion in subareas violates this boundary condition, and more so towards the edges of each subarea. Therefore, results from grains that intersect the subarea boundary are discarded after the inversion routine is performed. Grains that intersect the boundary and hence are partially in the subarea are, however, included in the inversion of that subarea to make sure their signal is not falsely attributed to other grains. Tiling also does have a major advantage. The magnetic moment of each individual grain is solved in multiple unique subareas, this enables a statistical analysis of the results. If the magnetic solution of a grain is robust, we expect only minor variations between the magnetic moments produced by the inversions of different subareas; if the results for a grain are dispersed, its solution is less accurate.

The inversion routine uses a least squares minimization to calculate the magnetic moment in three orthogonal directions per grain. The calculated magnetic moments and the spatial data from the grains are then used to create a calculated magnetic flux map at the surface in a forward model. This calculated magnetic flux map is subtracted from the original magnetic flux map to produce a map of the residuals, i.e. the measured magnetic signal that is not accounted for by the inversion.

3.5 Data processing

Tiling leads to multiple solutions for individual grains: on average there are 159 solutions per grain, with a minimum of 10 and a maximum of 225 solutions. From each individual solution (i.e. magnetic moment in three orthogonal components), the total magnetic moment, its declination with respect to the positive x-axis, and inclination with respect to the horizontal plane (downwards into the sample) are calculated. Also, for each individual solution, the distance to the nearest boundary for that grain in that subarea is determined. The entire dataset is subsequently grouped per grain; for each grain we determine its mean and median magnetic moments. Furthermore, the Fisher mean (Fisher 1953) is calculated, together with its precision parameter (k) and confidence interval (α95) for each grain. To assess the accuracy of the magnetic direction of each individual solution the angle between the Fisher mean for that grain and each of its individual solutions is determined (ΔAngle). It is important to note, however, that Fisher statistics only considers the directions of the magnetic moments, and not their magnitudes. To quantify the accuracy of the magnetic moment of each individual solution we calculate the percentual difference between the magnetic moment of each individual solution and the median magnetic moment for that grain (Δm). The ΔAngle and Δm proxies can be used to investigate the stability of the results per grain between solutions stemming from different subareas.

3.6 Mr/Ms ratio

To determine whether an allocated magnetic moment is reasonable, the allocated magnetic moment is divided by the theoretical maximum magnetic moment for that grain. The theoretical maximum magnetic moment is calculated based on the saturation magnetization of pure magnetite (480 kA/m, e.g. Dunlop and Özdemir 1997) and the volume of the grains as produced by the MicroCT analysis. This ratio is equal to the Mr/Ms ratio, as the volume factor that converts magnetic moment to magnetization is present in both the nominator and denominator and is a constant for an individual grain. The allocated magnetic moment can never be higher than this theoretical maximum, therefore results for which Mr/Ms >1 are inherently inaccurate. Since our grains have diameters >1.5-2 µm, they are firmly outside the single domain (SD) grainsize range for which a magnetic moment close to Mr/Ms = 1 can be expected. Realistic Mr/Ms values for individual grains are therefore well below 1, although there currently is no theoretical framework for their expected values. Furthermore, the mineralogical analyses showed that the iron-oxide grains are not pure magnetite, but titanomagnetite and ilmenite. Grains with a larger percentage of Ti may have three to four times lower Mr-values compared to magnetite (Dunlop and Özdemir 1997), and ilmenite does not hold a remanent magnetization at room temperature (Readman and O'Reilly 1972). To make it even more complex, parts of iron-oxide grains in our sample can be ilmenite while other parts are titanomagnetite (Ter Maat et al. 2018). This makes their 'magnetic grain size' smaller than the physical grain size as determined by MicroCT, lowering their expected Mr even further. All this implies that the calculated theoretical maximum magnetic moment is an absolute upper limit to the allocated magnetic moment by the inversion. For our grains it is safe to expect Mr/Ms values to be in the order of 0.1, and possibly even (much) lower.

3.7 Signal Strength Ratio

MMT's potential to accurately resolve a grain's magnetization depends on (1) the magnetic signal from that grain and (2) its distance to the surface of the magnetic scan (de Groot et al. 2018; 2021). Recently, Out et al. (2022) defined the signal strength ratio (SSR), a parameter that indicates the expected magnetic signal at the surface for each grain in the sample. It is based on the grain's depth in the sample (R), volume (V) and diameter (d) and calculated by: $SSR = \frac{V}{R^3 d}$. Furthermore, they numerically modelled the performance of MMT inversions as function of a grain's SSR and showed that the SSR can be used to select a subset of grains of which a pre-defined percentage of grains produces an accurately resolved magnetic moment. The proper SSR cut-off depends primarily on the noise in the magnetic scan and the concentration of grains in the sample (Out et al. 2022).

4. Results

We performed 16,874 MMT inversions to characterize the magnetic moments of 1,646 grains in our sample. Due to tiling of the subareas some grains were solved for more often than others, but 261,305 unique magnetic moments were obtained in total. Previous MMT studies were limited to samples or (sub)areas with <150 grains that were inverted only once (de Groot et al. 2018; 2021). Here we gain one order of magnitude in the number of grains that were analyzed and more than three orders of magnitude in the amount of unique magnetic moments that were obtained in a single MMT study. Below we first present results for individual grains, then for single subareas, and lastly consider the entire sample - including selecting the grains that are best resolved in our study.

4.1 Results for individual grains

As each grain is included in multiple unique subareas, the magnetic moment for each grain is determined between 10 and 225 times, with 159 times as average. In Fig. 3 we present the results for three typical grains in our sample that illustrate the differences in stability between the different MMT inversions. Grain 200 is poorly resolved: there are 225 solutions, but their directions are dispersed as indicated by a precision parameter k of 1.18 (Fig. 3a). Grain 319 performs better, with 180 solutions and a precision parameter of 5.63 (Fig. 3b). Grain 693 exhibits truly stable behavior with a k-value of 363.46 with 169 solutions (Fig. 3c). We see a similar trend in the inaccuracies of the magnitude of the magnetic moments. The Δm parameter that gives the percentual difference between an individual solution and the length of the median solution, shows a tight distribution around 0% for grain 693, and increasingly flatter distributions for grains 319 and 200, respectively (Fig. 3d). It is important to note, however, that the deviations in direction and magnitude are not linked one-to-one, i.e. not all solutions for which the direction is poorly resolved produce an inaccurate magnitude as well, and vice versa (Fig. 3e).

To generalize these three examples, we consider the distribution of k-values for the individual grains in our sample. Grain 319 is representative for the most common precision of the results for individual grains: the median k-value in the entire population is 4.17, with the first and third quartile being 2.43 and 9.57, respectively. The extremes are a grain with a k-value of 1.08 on the low end, and a grain with a k-value of 9,018.25 on the upper end.

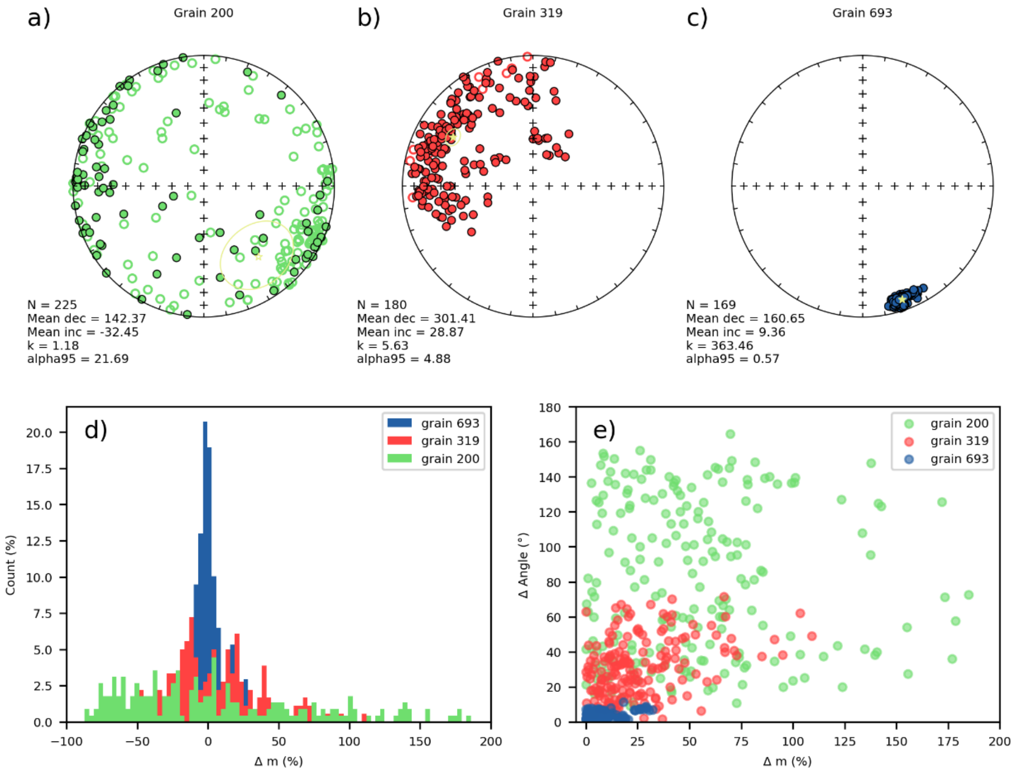

Figure 3 - Results for three typical grains. Panels a, b and c show the directional results in equal area projections for grains 200, 319 and 693 respectively; closed symbols are in the lower hemisphere corresponding to positive inclinations, open symbols are in the upper hemisphere with negative inclinations. The percentual deviation of individual magnetic moments with respect to the median magnetic moment for each grain (Δm) is in d. The relationship between the angular deviation (ΔAngle) and Δm for each individual solution is in e. Note that the x-axis in panels d and e is cut-off at 200% deviation; this excludes 19 individual solutions for grain 200 from the plots.

4.2. Results for an individual subarea

For each subarea the results consist of a list of calculated magnetic moments for the grains that are present in that subarea, a calculated map based on the forward model of the results produced by the inversion, and a map of the calculated residual field. The results of a typical subarea are presented in Fig. 4. It contains 22 grains that are fully within this subarea; another 3 are intersected by its boundary and are therefore included in the inversion, but their results are rejected. The list of solutions in this subarea are in Supplementary Table S1. The measured magnetic flux map shows one major expression that is not characteristically dipolar (Fig.6a, around [760,360]). Since our inversion only allocates dipoles to the individual grains, this anomaly is only partially resolved in the forward field (Fig. 6b) and leaves a distinct multipolar residual (Fig. 6c). The grain that is mainly beneath this multipole signal is grain 375, which is a large and shallow grain, from which multidomain behavior can be expected.

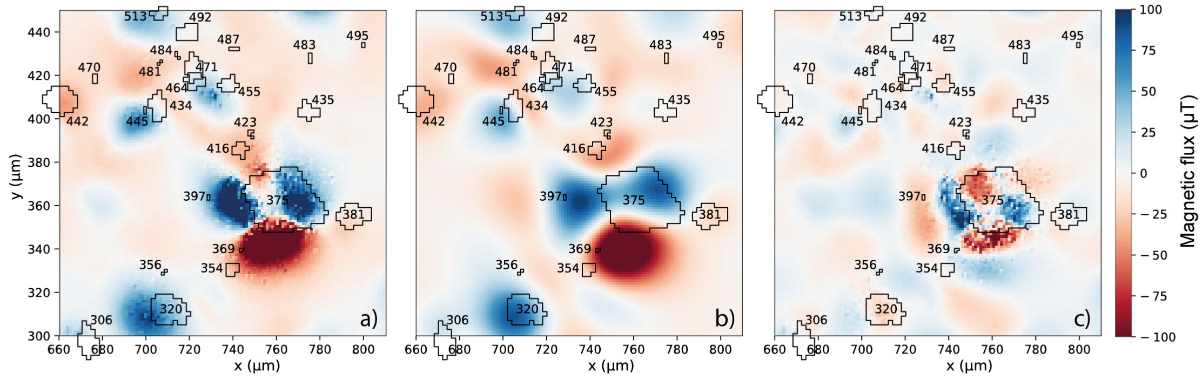

Figure 4 - Example of the results of a typical subarea; this subarea has its lower-left corner at [660,300] and its top-right corner at [810,450] in Fig. 3b. The measured magnetic flux is in panel a; the forward field based on the allocated magnetic moments in panel b; and the residual are in panel c. The grains in the subarea are outlined in black and indicated by their label (number).

Remarkably, the results for this grain are relatively robust between the inversions of different subareas in which this grain is present, as its results have a k-value of 28.43. For many other smaller grains, the residual is low indicating that the allocated magnetic moment is in line with the measured magnetic flux by the QDM.

4.3 Results for entire scanned surface

The overlapping field-of-view of the MicroCT and QDM scans encompasses 1,646 grains for which 261,305 unique magnetic moments were calculated in 16,874 subareas. We already showed that the results of some grains are more stable than others, so it is paramount to select only the most reliable magnetic moments. We therefore assess the results as function of (1) the theoretical remanence ratios (Mr/Ms) of the grains; (2) the distance to the closest boundary in the subarea; and (3) the SSR of the grains (Fig. 5). The Mr/Ms ratio has a theoretical maximum of 1, but accurate solutions of the remanent magnetization of grains in our sample are most likely in the order of 0.1 or less (section 3.6). Many solutions from our inversions have Mr/Ms ratios >1, but the SSR of these grains is generally low, and there is no trend between the Mr/Ms ratio of a solution and its distance to the closest boundary of the subarea (Fig. 5a). The accuracy of the direction of the magnetic moments does show a trend with distance to the closest boundary of the subarea (Fig. 5b). Apparently, missing parts of the magnetic expression of a grain does hamper a reliable determination of the direction more than the intensity. Again, the SSR is able to discriminate between accurate and less accurate results well, but the angular deviations are still in the order of tens of degrees, even for SSRs >0.1.

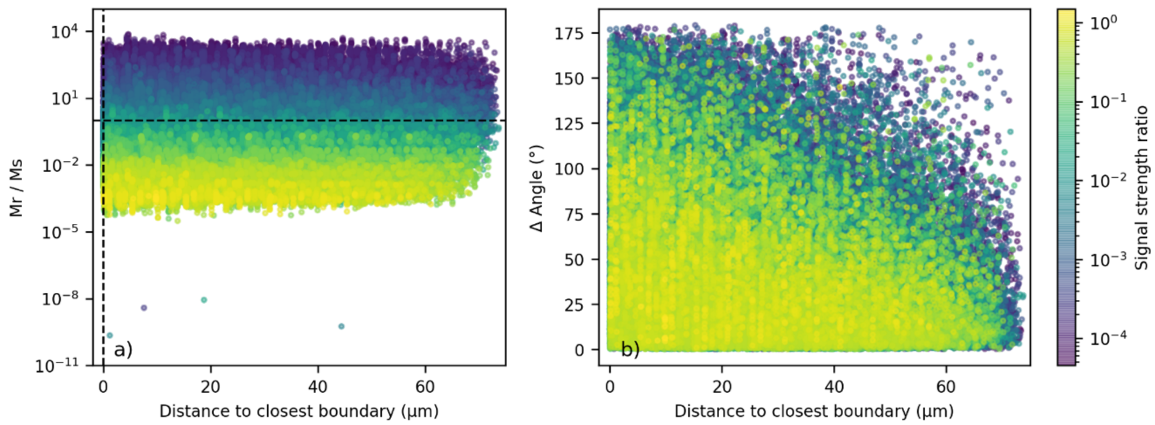

Figure 5 - Accuracy of the 261,305 uniquely determined magnetic moments from 1,646 grains as function of distance to closest boundary of the subarea and SSR. The accuracy is expressed as (theoretical) M_r/M_s ratio (a) which must be <1 and is most likely in the order of 0.1 or less; and as the angle between individual results and the mean direction of a grain (ΔAngle) in b. In both panels the results are color coded based on the SSR of the grain. Results with a theoretical M_r/M_s ratio >1 (indicated by the horizontal dashed line in a) are inaccurate as the allocated magnetization cannot be larger than the saturation magnetization.

5. Discussion

5.1 Mineralogy and grain sizes

The mineralogy of our sample was described in-depth by Ter Maat et al. (2018) and studied here (section 2). For our purposes only the iron-oxide grains in the sample are of interest, and they are abundant. To isolate the iron-oxides grains in the sample, we selected grains with high attenuation contrasts from the MicroCT scan. A high attenuation contrast is often interpreted as a material with a high density. Given the mineralogy of our sample it is likely that the vast majority of grains with a high density are iron-oxide grains. The spatial resolution of the MicroCT scan, however, limits the size of grains that are detected to >1.5-2 µm diameter. This means that iron-oxide grains with diameters <1.5-2 µm that are undoubtedly present in our sample are missed in our analyses. Moreover, the mineralogical study of our sample shows that the chemical composition of our iron-oxide grains varies from ilmenite to (titano-)magnetite. Since ilmenite does not carry a remanent magnetization at room temperature, not all iron-oxides in our sample will have a magnetic expression. Some grains even have mineralogical domains of which some are magnetic at room temperature while others are not. This implies that there are two major shortcomings in our MMT study: first, not all magnetic sources in the system are known, and second, some sources that are identified do not carry a remanent magnetization. It is difficult to assess the impact of these two shortcomings, and they are subject of ongoing research. We expect, however, that the impact of missing magnetic sources on the accuracy of MMT results is much larger than the impact of non-magnetic sources in the system. Missing a source directly violates the important boundary condition of the uniqueness theorem of the inversion that states that all, but only, the magnetic sources and magnetic signals in the system must be known (Fabian and de Groot 2019). Since the inversion can allocate a near-zero magnetic moment to a source in the system, including a non-magnetic source in the inversions seems to be a lesser issue. In future studies increasing the resolution of the MicroCT scan should be considered to identify as much of the iron-oxide grains in the sample as possible. The lower limit of 50 nm below which iron-oxide grains behave superparamagnetically (Dunlop and Özdemir 1997) is challenging but not impossible for current NanoCT scanners. The field-of-view of scanners with such resolutions, however, is often narrow, limiting the volume of the sample and hence the number of grains present in a scan.

Furthermore, the variation in mineralogy of the iron-oxides in our sample hampers our interpretation based on theoretical remanence ratios (Mr/Ms) that are based on the saturation magnetization (Ms) of pure magnetite (480 kA/m). First, the iron-oxide grains in our sample are large, multidomain, grains for which Mr/Ms ratios <<1 are expected. Second, the iron-oxide grains in our sample are titanomagnetites or ilmenites, instead of magnetites. Since titanomagnetite has a saturation magnetization three to four times lower than pure magnetite and ilmenite is paramagnetic at room temperature (e.g. Readman and O'Reilly 1972; Dunlop and Özdemir 1997), the expected Mr/Ms values are lowered even further. Third, some grains have mineralogical domains of both ilmenite and titanomagnetite. Their volume as identified by the MicroCT scan does not represent their 'magnetic volume' at room temperature. All this implies that the calculated Mr/Ms ratios are overestimated, and that the theoretical upper limit of 1 for the Mr/Ms ratios is too high. Therefore, we expect Mr/Ms values in the order of 0.1 or (much) less, although a theoretical framework for this value lacks.

5.2 Geometry of MMT experiments

A precise co-registration of the MicroCT and QDM datasets is paramount for the accuracy of MMT results. Small perturbations in the mapping between the two datasets may lead to increased uncertainties and/or poorly resolved grains in the MMT inversion. Also, the scan height –the sensor-sample distance that dictates the distance between the grains and the surface of the magnetic scan– needs to be known with precision, as errors in this distance propagate with the power of three in MMT results (de Groot et al. 2018).

In the current workflow the co-registration of the spatial data onto the magnetic surface scan is done by hand. This introduces an uncertainty in the mapping that may influence the results, although the grains do line up over the entire field-of-view of 1320x1570 µm, and there are no distortions evident over the surface (Fig. 2b). The optical image of the QDM greatly eases the mapping compared to the alignment of the MicroCT scan with magnetic anomalies in the Scanning SQUID Microscopy scan as was necessary in de Groot et al. (2018). Nevertheless, the mapping is time-consuming and sometimes difficult because it is done based on the geometry of shallow grains, which have a unique pattern, but which takes time to recognize in both the LED image from the QDM set-up and the surface grains from the MicroCT scan. We briefly explored the possibility of using pattern recognition software to map the surface grains to the LED image from the QDM-setup. The amount of data that the pattern recognition can use, however, is relatively scarce, because the MicroCT data consists of only the high-density grains. The results of the pattern recognition routine were not very promising, so currently, the tedious process of mapping the LED image of the QDM onto the shallow grains in the MicroCT scan by hand seems the most accurate way of co-registration.

5.3 Multidomain signals of large grains

The magnetic expression of large multidomain grains on the surface of the sample often is rather complex (e.g. grain 375 in Fig. 4a). Since the MMT inversion that we used here only solves for dipole magnetizations in a grain, it is likely that parts of the complex magnetization of such a multidomain grain are attributed to surrounding grains which are then assigned incorrect magnetizations. Even though the signal of these large multidomain grains may not be of interest for a paleomagnetic interpretation, solving them correctly would prevent their signal to be erroneously attributed to grains in their close surrounding. In a future study it is therefore worth exploring whether solving for non-dipolar behavior for large grains and/or grains that are close to the surface using the routines presented by Cortés-Ortuño et al. (2021) would improve the accuracy of MMT results. Special attention should be paid to select the best degree of the spherical harmonics for each grain; expanding the inversion to also solve non-dipole signals most likely increases the computational time considerably. Solving for higher order degrees of spherical harmonics introduces more variables per grain, reducing the amount of datapoints in the magnetic scan per variable to solve. Lastly, it would require a higher signal-to-noise ratio in the magnetic scan, since small errors can be accommodated in more detailed descriptions of a grain's magnetization, while they would be averaged out in a dipole approximation.

5.4 Effect of the subarea size

The subarea size is limited to 150x150 µm due to RAM memory requirements. The distance to the nearest subarea boundary influences the stability of the directional solution more than the stability of the length of the magnetic vector (Fig. 5). To explain the dependency of the stability of the solution to

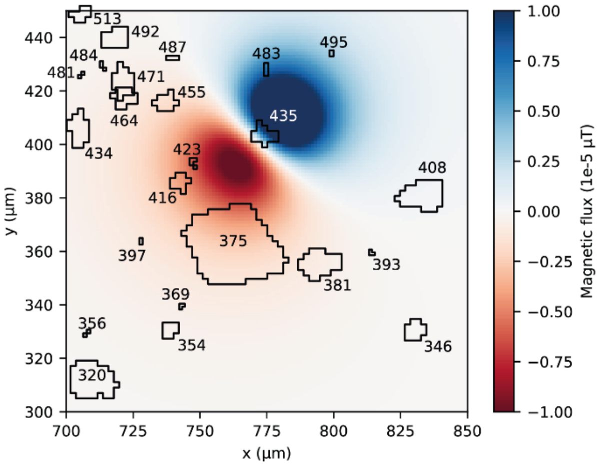

Figure 6 - The forward signal of grain 435 is present in a large part of the subarea. The contributions of the other grains are removed. Note that the color scale is exaggerated with respect to the other figures in this manuscript.

the distance to the closest boundary we determined the size of the surface area across which a single magnetic grain expresses its signal. We therefore calculated the forward signal of a small grain with a diameter of 2-3 μm (grain 435) while ignoring the magnetic signals of the surrounding grains (Fig. 6). Its magnetic signal on the surface is roughly circular with a diameter of 100 μm, it is therefore present in a major part of the subarea. Larger grains will exhibit even larger magnetic stray fields that encompass larger surface areas. This implies that when using 150x150 μm subareas (major) parts of the magnetic expressions of grains will be outside the subarea and are not considered in the inversion of that particular subarea. This violates a boundary condition of the uniqueness theorem that stipulates that all but only the magnetic sources and their magnetic signals in the system must be known (Fabian and de Groot 2019). It would therefore be desirable to work with larger subareas, or even invert for the entire sample at once. This will be pursued in a future study, when the computational limitations currently impeding larger (sub)areas are resolved.

5.5 Signal strength ratio cut-off

The signal strength ratio (SSR, Out et al. (2022)) provides an indication of the expected signal at the surface for each grain based on its size and location in the sample. The SSR is thus a first order estimate of the signal-to-noise ratio that can be expected for a grain, and as such an indication of how well the MMT inversion will be capable of solving its magnetic moment. Out et al. (2022) proposed to use SSR cut-offs above which MMT results can be trusted and illustrated that the SSR can be chosen such that a predefined percentage of the grains that are selected is accurate solved for by MMT.

Here we can test the performance of SSR cut-offs empirically on a natural sample for the first time. To determine the proper SSR cut-off for our dataset we consider the theoretical Mr/Ms ratios of the grains as function of their SSR (Fig. 7a). The SSR is governed by the volume of a grain and its depth in the sample, grains that are deeper in the sample and/or have a smaller volume have a lower SSR and are more difficult to resolve. SSR cut-offs of 0.01, 0.02, and 0.03 all eliminate almost all solutions with Mr/Ms >1. A SSR of ≥0.01 accepts some smaller but shallow grains that are poorly resolved – possibly because they are near larger grains for which the MMT assumption to solve for dipoles breaks down. A cut-off at 0.03 on the other hand rejects some larger, deeper grains that are properly resolved. A SSR of 0.02 therefore seems to be an optimal cut-off for our dataset (Fig. 7a). Remarkably, Out et al. (2022) predicted this SSR value ≥0.02 in one of their computational models that has corresponding characteristics to our natural sample in terms of grain density, noise level and scanning geometry. In the numerical model, this SSR selects a subset of grains of which 99% are solved within 1% of their known values. On the other hand, this SSR only selects 42.9% of the grains that did reproduce their magnetic moment in the numerical model; i.e. 57.1% of the grains that are properly resolved by the inversion were unfortunately rejected.

In our sample, a SSR of ≥0.02 contains 419 grains (Fig 7b). Only one of these grains has results for which Mr/Ms ≥1, namely grain 1870. Inspection of this grain shows that this is most likely a portion of a larger grain that was not completely imaged by the MicroCT scan. It has a very small volume (3.4 μm^3 or 11 voxels), and there are two other grains very close to it. For the directional results the SSR ≥0.02 eliminates results over the whole range of the dataset (Fig 7c). However, when comparing Fig. 5b (directional scatter for all grains) and Fig. 7c (directional scatter for grains with an SSR ≥0.02) it is evident that the cut-off value does reject many grains with a high angular deviation. To assess the performance of using the SSR as cut-off further, we determined the median ∆Angle and Δm parameters, and the precision parameter k, for the entire set of solutions (1,646 grains) and the solutions that are associated with an SSR ≥0.02 (419 grains). The median ∆Angle changes from 25.0° to 17.8°, the median Δm goes from 22.7% to 15.2%, and the median k changes from 4.17 to 8.07. This illustrates that the SSR cut-off indeed selects grains that exhibit more stable behavior in the inversions of the different subareas in which it is included, and that the SSR is a powerful tool to scrutinize MMT results from natural samples.

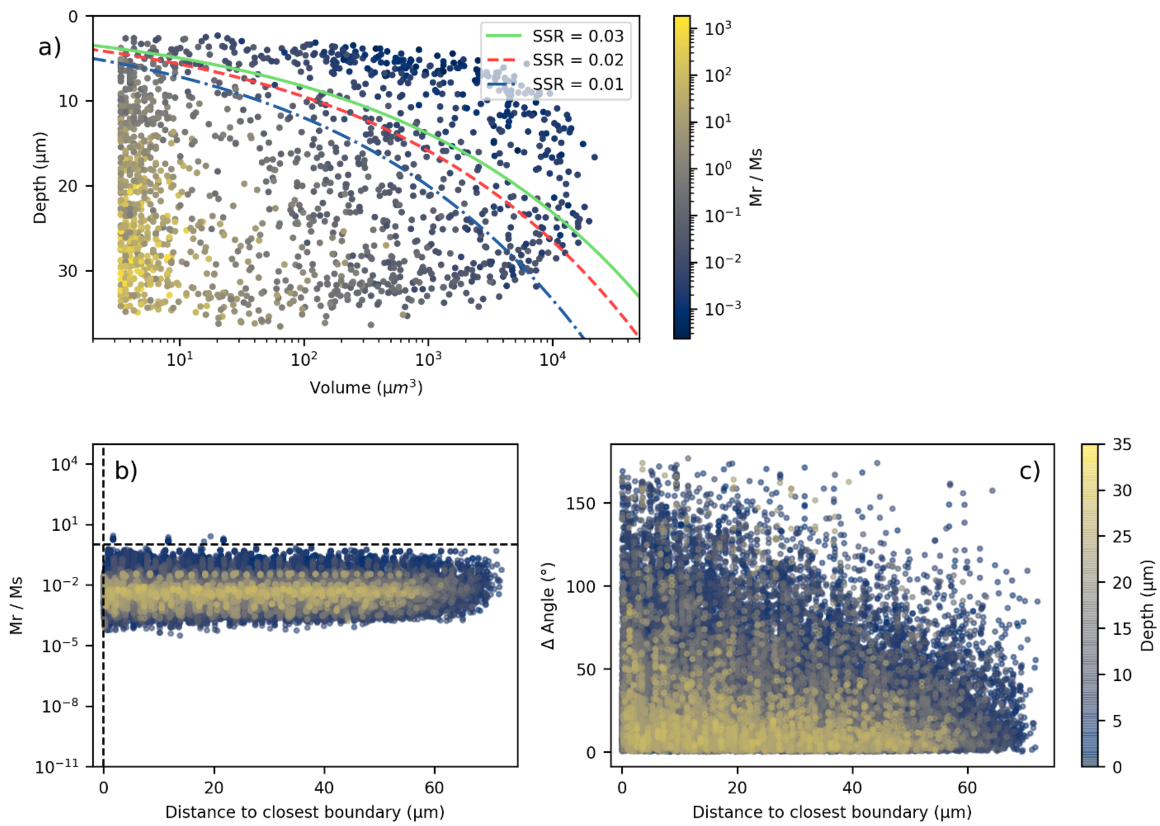

Figure 7 - The SSR is a powerful tool to select MMT. In a the Mr/Ms ratio for each grain present in the sample is indicated as function of its volume and depth in the sample; three SSR cut-offs are indicated and show which grains are selected. The grains with a SSR ≥0.02 are In b and c; the Mr/Ms ratio (b) and ΔAngle (c) are given as function of distance to closest boundary and color coded by their depth in the sample. Panels b and c are similar to panels a and b in Fig. 5, but only show data points with a SSR ≥0.02.

5.6 Paleomagnetic interpretation

The paleomagnetic potential of MMT is based on the assumption that a certain subset of grains in a sample contains the reliable remanent signal that is indicative of the past state of Earth's magnetic field. Beyond SD grains, for which (Berndt et al. 2016) provided important boundary conditions, it is enigmatic which grains are reliable recorders of the paleofield and if so, how many of such grains are necessary to provide a meaningful statistical ensemble for a paleomagnetic interpretation. Grains in the PSD realm (<1 µm) get increasingly more attention as possible stable recorders because of their potential vortex states (e.g. Nagy et al. 2017; 2019). Multidomain grains are often regarded as unreliable recorders over (geologic) time scales (e.g. de Groot et al. 2014). The detection limit of the MicroCT scan used here (>1.5-2 µm) only allows to characterize large, MD, grains in our sample. This implies that we miss gains that are of SD or PSD nature –the grains that are often believed to be more reliably recorders of the Earth's paleofield– in our study. In future studies the resolution of the MicroCT scan must be lowered by approximately one order of magnitude, before a meaningful

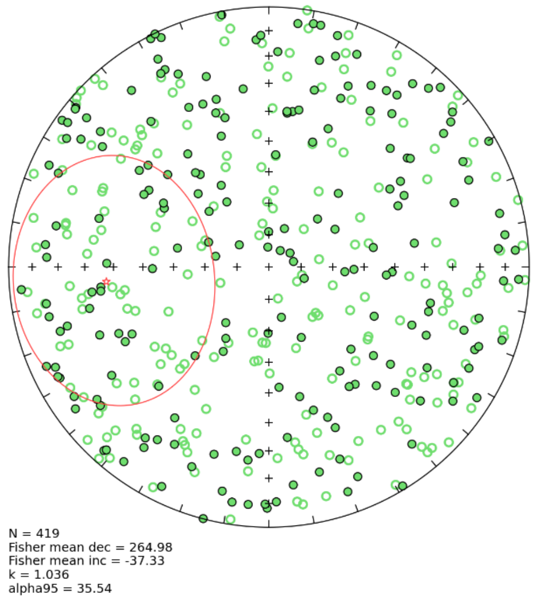

Figure 8 - The mean directions of 419 grains with a SSR ≥0.02 in an equal area projection; closed symbols are in the lower hemisphere corresponding to positive inclinations, open symbols are in the upper hemisphere with negative inclinations. The Fisher mean of these grains is indicated by a red star, together with its 95% confidence interval as red line.

paleomagnetic interpretation of MMT results will. be possible. Technically, resolutions <500 µm are already achievable in NanoCT/MicroCT scans, but such scans have a limited field-of-view, lowering the amount of grains in the scan. Therefore the 'sweet-spot' in the trade-off between field-of-view and MicroCT resolution should be determined by the research question and the physical characteristics of the sample material to optimize the paleomagnetic interpretation of MMT results.

Although an interpretation in paleomagnetic terms is not possible, we can use the MMT solutions of the grains that have a SSR ≥0.02 to calculate their dispersion in directions. Since all grains analyzed in our study underwent the same magnetic history since solidification, their magnetizations are expected to be the result of the same external magnetic field(s). Their magnetic dispersion therefore gives a first-order estimate of how many large, MD, grains would be necessary to produce a consistent paleomagnetic direction. The Fisher mean for the 419 grains with a SSR ≥0.02 gives a declination of 265.0° and an inclination of -37.3°, with a precision parameter k of 1.036 and confidence interval α_{95} of 35.5° (Fig. 8). As the number of grains, the precision parameter and the confidence interval are related (e.g. Butler 1992), the number of grains required to get a smaller confidence interval with the current precision parameter can be calculated. An uncertainty of 10° or less is often considered reliable (Berndt et al. 2016); this implies that given on our k of 1.036, 5,430 grains would be required to attain a confidence interval of 10°. This is 12.9 times more than the current dataset of 419 grains. Our 419 grains are produced by a scanned surface of 1.52 mm^2. To acquire data from 5,430 grains after applying our MMT inversion and SSR cut-off a scan surface of 19.6 mm^2 would be required. This is in remarkable agreement with the prediction by de Groot et al. (2021) that scanning an area of 20 mm^2 would be necessary for a 'reliable' result in a volcanic sample, although it must be emphasized again that the MD grains in or our analyses are most likely not reliable paleomagnetic recorders, at least not on geological timescales.

6. Conclusion

We presented a large-scale application of MMT on a natural sample producing magnetic moments of 1,646 individual grains in our sample. Due to tiling in our inversion routine, we obtained on average 159 magnetic moments for each grain, so our study produced 261,305 individual magnetic moments in total. This enabled a statistical assessment of the results using the recently proposed signal strength ratio. After selecting the most reliable MMT results using a SSR cut-off of 0.02, we obtained robust results for 419 rather large and/or very shallow grains in our sample. Previous MMT studies produced magnetic moments for <150 grains. We therefore gain one order of magnitude in the number of grains that were analyzed and more than three orders of magnitude in the amount of unique magnetic moments that were obtained in a single MMT study. The most important recommendation that arises from our findings is that samples for MMT studies should be smaller than the sample with a diameter of 3 mm that we used here. If the diameter of the sample would be in the order of 1 mm it would be possible to (1) measure the magnetization of the entire surface in one QDM scan, and (2) fit the sample in the field-of-view of MicroCT scanners with resolutions <500 nm. This would imply that we could determine the magnetic moments of smaller (< 1 µm) grains that may exhibit PSD behavior and are therefore better paleomagnetic recorders than the MD grains we currently can analyze. Also, if a better optimization of the MMT inversion would allow to invert the magnetic scan of such a 1 mm sample at once, we would satisfy the boundary condition of the MMT inversion theory that all, but only, magnetizations arising from the sources in the sample must be measured. This would remove the need for tiling during the MMT analyses and undoubtedly lead to better MMT results. Nevertheless, our study is an important step towards making MMT a useful paleomagnetic and rock-magnetic technique.

Data statement

The data used in this study has been uploaded to the Pangaea.de repository and will be available soon. Pending the FAIR data check by Pangaea we uploaded the data for peer review.

Acknowledgements

The authors declare no competing interests. This project has received funding from the European Research Council (ERC) under the European Union's Horizon 2020 research and innovation programme (Grant agreement No. 851460 ‘MIMATOM’ to LVdG). LVdG acknowledges funding from the Dutch Science Foundation (NWO) grant ALWOP.641.

References

Almeida, Trevor P., Adrian R. Muxworthy, András Kovács, Wyn Williams, Paul D. Brown, and Rafal E. Dunin-Borkowski. 2016. “Direct Visualization of the Thermomagnetic Behavior of Pseudo-Single-Domain Magnetite Particles.” *Science Advances* 2 (4): e1501801. https://doi.org/10.1126/sciadv.1501801.

Berndt, Thomas, Adrian R. Muxworthy, and Karl Fabian. 2016. “Does Size Matter? Statistical Limits of Paleomagnetic Field Reconstruction from Small Rock Specimens.” *Journal of Geophysical Research: Solid Earth* 121 (1): 15–26. https://doi.org/10.1002/2015JB012441.

Butler, Robert F. 1992. *Paleomagnetism : Magnetic Domains to Geologic Terranes*. *Paleomagnetism : Magnetic Domains to Geologic Terranes*. Boston: Blackwell Scientific Publications.

Cortés-Ortuño, David, Karl Fabian, and Lennart V. de Groot. 2021. “Single Particle Multipole Expansions From Micromagnetic Tomography.” *Geochemistry, Geophysics, Geosystems* 22 (4). https://doi.org/10.1029/2021GC009663.

Dunlop, David J., and Özden Özdemir. 1997. *Rock Magnetism*. Cambridge: Cambridge University Press. https://doi.org/10.1017/CBO9780511612794.

Egli, Ramon, and Friedrich Heller. 2000. “High-Resolution Imaging Using a High-Tc Superconducting Quantum Interference Device (SQUID) Magnetometer.” *Journal of Geophysical Research: Solid Earth* 105 (B11): 25709–27. https://doi.org/10.1029/2000jb900192.

Fabian, Karl, and Lennart V. de Groot. 2019. “A Uniqueness Theorem for Tomography-Assisted Potential-Field Inversion.” *Geophysical Journal International* 216 (2): 760–66. https://doi.org/10.1093/gji/ggy455.

Farchi, E., Yael Ebert, D. Farfurnik, G. Haim, R. Shaar, and N. Bar-Gill. 2017. “Quantitative Vectorial Magnetic Imaging of Multi-Domain Rock Forming Minerals Using Nitrogen-Vacancy Centers in Diamond.” *SPIN* 07 (03): 1740015. https://doi.org/10.1142/S201032471740015X.

Feinberg, Joshua M., Richard J. Harrison, Takeshi Kasama, Rafal E. Dunin-Borkowski, Gary R. Scott, and Paul R. Renne. 2006. “Effects of Internal Mineral Structures on the Magnetic Remanence of Silicate-Hosted Titanomagnetite Inclusions: An Electron Holography Study.” *Journal of Geophysical Research: Solid Earth* 111 (12): 1–11. https://doi.org/10.1029/2006JB004498.

Fisher, R.A. 1953. “Dispersion on a Sphere.” *Proceedings of the Royal Society A: Mathematical, Physical and Engineering Sciences* 217 (1130): 295–305. https://doi.org/10.1098/rspa.1953.0064.

Fu, Roger R., Eduardo A. Lima, Michael W. R. Volk, and Raisa Trubko. 2020. “High-Sensitivity Moment Magnetometry With the Quantum Diamond Microscope.” *Geochemistry, Geophysics, Geosystems* 21 (8): 1–17. https://doi.org/10.1029/2020GC009147.

Glenn, D. R., R. R. Fu, P. Kehayias, D. Le Sage, Eduardo A. Lima, B. P. Weiss, and R. L. Walsworth.

2017. “Micrometer-Scale Magnetic Imaging of Geological Samples Using a Quantum Diamond Microscope.” *Geochemistry, Geophysics, Geosystems* 18 (8): 3254–67. https://doi.org/10.1002/2017GC006946.

Groot, Lennart V. de, Andrew J. Biggin, Mark J. Dekkers, Cor G. Langereis, and Emilio Herrero-Bervera. 2013. “Rapid Regional Perturbations to the Recent Global Geomagnetic Decay Revealed by a New Hawaiian Record.” *Nature Communications* 4 (1): 2727. https://doi.org/10.1038/ncomms3727.

Groot, Lennart V. de, Karl Fabian, Iman A. Bakelaar, and Mark J. Dekkers. 2014. “Magnetic Force Microscopy Reveals Meta-Stable Magnetic Domain States That Prevent Reliable Absolute Palaeointensity Experiments.” *Nature Communications* 5 (1): 4548. https://doi.org/10.1038/ncomms5548.

Groot, Lennart V. de, Karl Fabian, Annemarieke Béguin, Pim Reith, Auke Barnhoorn, and Hans Hilgenkamp. 2018. “Determining Individual Particle Magnetizations in Assemblages of Micrograins.” *Geophysical Research Letters* 45 (7): 2995–3000. https://doi.org/10.1002/2017GL076634.

Groot, Lennart V., Karl Fabian, Annemarieke Béguin, Martha E. Kosters, David Cortés-Ortuño, Roger R. Fu, Chloë M. L. Jansen, Richard J. Harrison, Tristan Leeuwen, and Auke Barnhoorn. 2021. “Micromagnetic Tomography for Paleomagnetism and Rock-Magnetism.” *Journal of Geophysical Research: Solid Earth* 126 (10): 1–21. https://doi.org/10.1029/2021JB022364.

Harrison, Richard J., Rafal E. Dunin-Borkowski, and Andrew Putnis. 2002. “Direct Imaging of Nanoscale Magnetic Interactions in Minerals.” *Proceedings of the National Academy of Sciences of the United States of America* 99 (26): 16556–61. https://doi.org/10.1073/pnas.262514499.

Levine, Edlyn V., Matthew J. Turner, Pauli Kehayias, Connor A. Hart, Nicholas Langellier, Raisa Trubko, David R. Glenn, Roger R. Fu, and Ronald L. Walsworth. 2019. “Principles and Techniques of the Quantum Diamond Microscope.” *ArXiv*.

Lima, Eduardo A., and Benjamin P. Weiss. 2009. “Obtaining Vector Magnetic Field Maps from Single-Component Measurements of Geological Samples.” *Journal of Geophysical Research* 114 (B6): B06102. https://doi.org/10.1029/2008JB006006.

Lima, Eduardo A., and Benjamin P. Weiss. 2016. “Ultra-High Sensitivity Moment Magnetometry of Geological Samples Using Magnetic Microscopy.” *Geochemistry, Geophysics, Geosystems* 17 (9): 3754–74. https://doi.org/10.1002/2016GC006487.

Maat, Geertje W. Ter, Gillian M. Pennock, and Lennart V. de Groot. 2018. “Data Descriptor: A Chemical, Crystallographic and Magnetic Characterisation of Individual Iron-Oxide Grains in Hawaiian Lavas.” *Scientific Data* 5: 1–9. https://doi.org/10.1038/sdata.2018.162.

Nagy, Lesleis, Wyn Williams, Adrian R. Muxworthy, Karl Fabian, Trevor P. Almeida, Pádraig Ó Conbhuí, and Valera P. Shcherbakov. 2017. “Stability of Equidimensional Pseudo–Single-Domain Magnetite over Billion-Year Timescales.” *Proceedings of the National Academy of Sciences* 114 (39): 10356–60. https://doi.org/10.1073/pnas.1708344114.

Nagy, Lesleis, Wyn Williams, Lisa Tauxe, and Adrian R. Muxworthy. 2019. “From Nano to Micro: Evolution of Magnetic Domain Structures in Multi-domain Magnetite.” *Geochemistry, Geophysics, Geosystems*, no. May: 1–12. https://doi.org/10.1029/2019gc008319.

Nichols, Claire I.O., James F.J. Bryson, Julia Herrero-Albillos, Florian Kronast, Francis Nimmo, and Richard J. Harrison. 2016. “Pallasite Paleomagnetism: Quiescence of a Core Dynamo.” *Earth and Planetary Science Letters* 441 (May): 103–12. https://doi.org/10.1016/j.epsl.2016.02.037.

Out, Frenk, David Cortés-Ortũno, Karl Fabian, Tristan Leeuwen, and Lennart V. Groot. 2022. “A First-order Statistical Exploration of the Mathematical Limits of Micromagnetic Tomography.” *Geochemistry, Geophysics, Geosystems*. https://doi.org/10.1029/2021gc010184.

Readman, P. W., and W. O’Reilly. 1972. “Magnetic Properties of Oxidized (Cation-Deficient) Titanomagnetites (Fe, Ti, □)3O4.” *Journal of Geomagnetism and Geoelectricity* 24 (1): 69–90. https://doi.org/10.5636/jgg.24.69.

Sakellariou, A., T.J. Sawkins, T.J. Senden, and A. Limaye. 2004. “X-Ray Tomography for Mesoscale Physics Applications.” *Physica A: Statistical Mechanics and Its Applications* 339 (1–2): 152–58. https://doi.org/10.1016/j.physa.2004.03.055.

Tauxe, Lisa, and Toshitsugu Yamazaki. 2015. “Paleointensities.” In *Treatise on Geophysics*, 461–509. Elsevier. https://doi.org/10.1016/B978-0-444-53802-4.00107-X.

Weiss, Benjamin P., Eduardo A. Lima, Luis E. Fong, and Franz J. Baudenbacher. 2007. “Paleomagnetic Analysis Using SQUID Microscopy.” *Journal of Geophysical Research: Solid Earth* 112 (9): B09105. https://doi.org/10.1029/2007JB004940.

AGU PUBLICATIONS

G-Cubed

Supporting Information for

Unravelling the magnetic signal of individual grains in a Hawaiian lava using Micromagnetic Tomography

Martha E. Kosters[1], Rosa A. de Boer[1], Frenk Out[1], David I. Cortés-Ortuño[1], and Lennart V. de Groot[1]

[1]Utrecht University

Contents of this file

Supplementary Table S1

Introduction

This supplementary information contains one supplementary table.

Caption table S1. Table showing results for a single subarea with coordinates (300, 660)(450, 810) (x0, y0)(x1,y1). The Raw data is the magnetic moment in three components as is produced by the inversion of this subarea. From this the magnetic moment is calculated. For each grain the results from subareas in which the grain was fully in the FOV are compiled separately from which a median result is extracted. The Δm is the percentual difference between the individual result and the median result of that specific grain. Mr/Ms is the calculated ratio of the individual result divided by the maximum magnetic moment for that specific grain. The directional results contains firstly the two columns with the declination and inclination of that individual solution. Then next two columns contain the Fisher mean declination and inclination that was calculated from the compiled results per grain, based on n solutions, with corresponding k and α95 (all specific to a certain grain). ΔAngle then is the number of degrees between the individual direction (dec, inc) and the Fisher mean (dec,inc) for that grain. Lastly a number of physical properties are listed that are specific for the individual grains, such as depth (R), volume (V), the number of voxels the grain consists of (# voxels), the calculated diameter (assuming the volume is a perfect sphere), the signal strength ratio (SSR), the saturation magnetic moment and the distance to the closest boundary for that specific grain in that specific subarea.

	Raw data			Magnetic results			Directional results								Physical properties						
Grain	Mx (A m2)	My (A m2)	Mz (A m2)	Magn. moment (A m2)	Δm (%)	Mr/Ms	Declination (°)	Inclination (°)	Fisher Decl (°)	Fisher Incl (°)	n	k	α95 (°)	ΔAngle (°)	R (µm)	V (µm^3)	# voxels	Diameter (µm)	SSR (/µm)	Saturation Magn (Am2)	Distance to boundary (µm)
320.00	-4.301E+06	-8.310E+06	-2.019E+07	2.225E+07	13.241	2.790E-02	207.37	-65.13	227.00	-32.91	182	10.674	3.356	34.36	23.24	1661.68	5403.00	14.70	9.01E-03	7.976E+08	2.02
346.00	-2.080E+06	-3.158E+06	-8.801E+05	3.883E+06	16.929	2.939E-02	213.37	-13.10	206.00	-14.81	196	30.595	1.848	7.36	17.35	275.25	895.00	8.07	6.53E-03	1.321E+08	15.08
354.00	9.465E+07	-2.001E+07	-7.191E+07	1.205E+08	44.111	2.057E+00	101.94	-36.62	106.61	-26.92	196	6.276	4.377	10.47	30.54	122.10	397.00	6.16	6.97E-04	5.861E+07	27.40
356.00	-1.473E+07	4.334E+07	-1.579E+07	4.842E+07	51.048	2.050E+01	341.23	-19.03	330.94	-15.91	210	1.607	12.445	10.30	33.71	4.92	16.00	2.11	6.09E-05	2.362E+06	6.73
369.00	-6.437E+07	4.884E+07	4.543E+07	9.270E+07	18.900	3.925E+01	307.19	29.34	302.05	25.27	210	12.643	2.846	6.12	25.19	4.92	16.00	2.11	1.46E-04	2.362E+06	38.32
375.00	4.704E+06	7.623E+06	-3.880E+06	9.762E+06	9.404	1.852E-03	31.68	-23.42	34.78	-32.17	132	28.433	2.344	9.17	12.97	10978.50	35697.00	27.57	1.82E-01	5.270E+09	43.37
381.00	4.757E+04	-8.942E+03	1.719E+05	1.786E+05	28.385	4.801E-04	100.65	74.28	359.56	78.95	169	2.335	9.367	20.81	6.70	775.02	2520.00	11.40	2.26E-01	3.720E+08	46.74
393.00	2.284E+05	4.884E+05	1.613E+05	5.627E+05	55.815	3.177E-01	25.06	16.65	3.44	18.21	210	1.872	10.388	20.67	17.46	3.69	12.00	1.92	3.62E-04	1.771E+06	34.36
397.00	4.002E+07	3.237E+07	-1.100E+07	5.264E+07	52.206	2.972E+01	51.03	-12.06	75.22	-26.19	225	9.262	3.263	26.78	27.65	3.69	12.00	1.92	9.11E-05	1.771E+06	27.73
408.00	1.060E+06	8.044E+04	-1.370E+06	1.734E+06	40.123	4.657E-03	85.66	-52.18	44.86	-49.68	182	1.924	10.842	25.49	32.25	775.63	2522.00	11.40	2.03E-03	3.723E+08	9.12
416.00	2.789E+05	7.003E+05	-4.096E+05	8.579E+05	6.649	9.784E-03	21.71	-28.52	9.41	-7.76	210	4.164	5.458	23.78	6.08	182.68	594.00	7.04	1.16E-01	8.769E+07	39.14
423.00	9.584E+06	4.873E+07	9.955E+06	5.065E+07	55.204	8.169E+00	11.13	11.34	21.91	40.87	225	2.730	7.128	31.02	25.35	12.92	42.00	2.91	2.72E-04	6.200E+06	46.53
434.00	-3.096E+06	-9.843E+05	-2.421E+05	3.258E+06	8.078	2.174E-02	252.36	-4.26	269.26	53.12	195	1.606	12.920	59.12	12.07	312.16	1015.00	8.42	2.11E-02	1.498E+08	0.57
435.00	1.791E+06	1.871E+06	-6.235E+05	2.664E+06	13.465	2.442E-02	43.74	-13.54	348.00	-6.73	196	1.859	10.835	55.18	18.76	227.28	739.00	7.57	4.55E-03	1.091E+08	40.93
455.00	-1.122E+07	4.660E+05	-3.915E+06	1.189E+07	62.212	1.492E-01	272.38	-19.22	246.21	-0.79	196	3.755	6.055	31.58	15.01	166.08	540.00	6.82	7.20E-03	7.972E+07	29.48
464.00	-2.030E+07	-3.461E+06	-5.279E+06	2.126E+07	68.352	1.461E-01	260.33	-14.38	324.15	-39.16	196	1.628	12.665	60.78	17.46	303.24	986.00	8.34	6.83E-03	1.456E+08	16.81
471.00	1.511E+05	4.023E+05	-1.829E+05	4.670E+05	33.131	3.268E-03	20.58	-23.05	275.75	14.82	182	1.882	11.101	109.14	5.02	297.71	968.00	8.28	2.83E-01	1.429E+08	17.46
481.00	-8.759E+07	2.187E+07	8.796E+07	1.260E+08	251.834	7.115E+01	284.02	44.26	47.83	60.94	225	2.092	8.968	65.39	31.67	3.69	12.00	1.92	6.06E-05	1.771E+06	4.81
483.00	4.984E+06	2.904E+07	5.139E+06	2.991E+07	62.599	4.824E+00	9.74	9.89	42.40	35.22	210	3.698	5.911	39.05	32.07	12.92	42.00	2.91	1.35E-04	6.200E+06	19.63
484.00	-1.586E+06	-5.503E+05	-4.769E+05	1.745E+06	36.580	6.953E-01	250.86	-15.86	306.92	32.94	210	2.869	7.099	72.41	8.75	5.23	17.00	2.15	3.63E-03	2.510E+06	12.96
487.00	-1.618E+07	-1.866E+07	-3.070E+07	3.940E+07	45.833	6.510E+00	220.92	-51.18	184.66	-2.50	210	2.121	9.163	57.39	32.01	12.61	41.00	2.89	1.33E-04	6.053E+06	16.90
492.00	-2.669E+06	-4.835E+06	-1.349E+07	1.458E+07	59.889	7.447E-02	208.89	-67.74	16.77	-12.15	196	1.862	10.816	99.63	21.22	407.81	1326.00	9.20	4.64E-03	1.957E+08	6.01
495.00	-1.512E+06	-3.61E+06	3.407E+06	5.189E+06	8.924	2.929E+00	202.73	41.04	154.97	70.78	196	4.138	5.481	38.11	24.40	3.69	12.00	1.92	1.32E-04	1.771E+06	14.86